CrossMark
click for updates

First principles calculations, neutron, and x-ray diffraction investigation of $Y_3Ni_{13}B_2$, $Y_3Co_{13}B_2$, and $Y_3Ni_{10}Co_3B_2$

N. Plugaru,[1] M. Valeanu,[1] R. Plugaru,[2,a)] and J. Campo[3]

[1]*National Institute of Materials Physics, Atomistilor Str. 105bis, Magurele-Bucharest 077125,*
P.O. Box MG-07, Ilfov, Romania
[2]*National Institute for R&D in Microtechnologies, Erou Iancu Nicolae Str. 126A, Bucharest 077190,*
P.O. Box 38-160, Romania
[3]*Material Science Institute of Aragon, University of Zaragoza, C.S.I.C., E-50009 Zaragoza, Spain*

Fully relativistic calculations within the local spin density approximation and the generalized gradient approximation were performed to determine the local spin and orbital magnetic moments, as well as the magnetocrystalline anisotropy energy of $Y_3Ni_{13}B_2$, $Y_3Co_{13}B_2$, and $Y_3Ni_{10}Co_3B_2$ compounds. A weak in-plane magnetic anisotropy is determined for $Y_3Ni_{13}B_2$, under the assumption of a crystallographic-like magnetic unit cell and collinear magnetic moments. The calculations predict considerable c-axis anisotropy for $Y_3Co_{13}B_2$ and $Y_3Ni_{10}Co_3B_2$, but smaller than that of YCo_5. The values of the magnetocrystalline anisotropy energy correlate well with both the magnitude of the orbital magnetic moment and the orbital magnetic moment anisotropy. The mixing between Co or Ni 3d states and B 2p states, observable at the bottom of the valence band of the 3d metal having a boron atom nearest neighbor, decreases the 3d spin and especially, the 3d orbital magnetic moments. $Y_3Ni_{13}B_2$ and $Y_3Ni_{10}Co_3B_2$ were also investigated by powder neutron diffraction experiments, at temperatures between 1.8 and 249 K. The Co and Ni site averaged magnetic moments calculated in the mixed compound are in fair agreement with the values obtained by the refinement of the magnetic contribution to the diffraction pattern. © 2014 AIP Publishing LLC. [http://dx.doi.org/10.1063/1.4862163]

I. INTRODUCTION

The hexagonal compounds in the $R_{m+n}T_{5m+3n}B_{2n}$ series, where $T = Co$ or Ni,[1,2] have attracted much interest mainly due to the exceptional hard magnetic properties of $SmCo_5$ and YCo_5 (m = 1, n = 0).[3,4] Thus, $SmCo_z$ (z = 5–8.5) based magnets still set the reference for high temperature applications, see, for example, Refs. 5–8. YCo_5 exhibits a remarkably high anisotropy energy, 3.86 meV/f.u. at 4.2 K,[9] which is about one quarter of the magnetocrystalline anisotropy energy (MAE) of the Sm compound.[10] An impressive research effort has been undertaken on the 1:5 phases to tailor their hard magnetic properties for applications, and on the fundamental side, to reveal the origin of the outstanding magnetic anisotropy of the essentially itinerant Co 3d electrons. Actually, YCo_5 has become a real workbench for the study of the 3d orbital polarization,[11,12] as well as for the *ab initio* calculations of MAE and orbital magnetic moment.[13–20]

At the same time, taking advantage of the structural regularity of the $R_{m+n}T_{5m+3n}B_{2n}$ series, the researches have extended over various stabilized stoichiometries, particularly with m = 1 and n = 1, 2, 3, and infinity. Thus, neutron diffraction experiments performed on $R_{n+1}Co_{3n+5}B_{2n}$ (n = 1, 2, 3 and infinity) have brought evidence on (i) the preferential occupation character of the 3d metal sites;[21,22] (ii) the dependence of the local cobalt magnetic moments on the

details of the local environment, particularly on the presence of B atoms nearest neighbors (n.n.),[23,24] and (iii) the reduction of exchange field at the R site due to the Co magnetic moment decrease in the boron containing phases, with respect to RCo_5.[25] X-ray magnetic circular dichroism (XMCD) measurements performed at the Co K edge in YCo_4B revealed a decrease in the amplitude of the XMCD signal relative to that of $LaCo_5$, which was attributed to the decrease in both the purely atomic contribution and the contribution of the spin–orbit interaction.[26] The *ab initio* electronic structure and the effect of boron on the elastic properties of $Y_{n+1}Co_{3n+5}B_{2n}$ (n = 1, 2, 3, infinity) were also reported.[27]

The $R_3T_{13}B_2$ compounds (m = 2, n = 1) have arisen interest because they could benefit of the attractive magnetic properties of the 1:5 phase in a superstructure containing a smaller fraction of boron than the m = 1 series.[28–34] An overview of the yttrium based systems shows that ferromagnetism (FM) with a Curie temperature of 65 K was firstly reported for $Y_3Ni_{13}B_2$.[35] Then, results of a thorough investigation by x-ray diffraction and magnetic measurements of $Y_3Ni_{13-x}Co_xB_2$, with x ≤ 5, were presented in Ref. 36 and the T-x magnetic phase diagram was elaborated. It was suggested that $Y_3Ni_{13}B_2$ is an uncompensated itinerant antiferromagnet (AFM) with coupled FM and AFM modes up to a Néel temperature of 68 ± 2 K. A paramagnetic temperature $\theta_p = 76$ K and a nickel effective magnetic moment $\mu_{eff} = 0.71 \mu_B$/Ni at. were also reported.[36] $Y_3Ni_{10}Co_3B_2$ was found to order ferromagnetically with a Curie temperature of 170 ± 2 K and a magnetic moment of 2.39 μ_B/f.u. at 5 K. To

a)Author to whom correspondence should be addressed. Electronic mail: rodica.plugaru@imt.ro

date, no magnetic data have been reported for $Y_3Co_{13}B_2$, which eludes the synthesis in single phase form.[36]

The 3:13:2 unit cell, depicted in Figure 1, consists of two 1:5 slabs (m = 2) and one 1:3:2 slab (n = 1).[2] The 3d metal sites, 2c and 3g in the 1:5 structure, are structurally related to the (2c, 4h) and (3g, 6i) sites, respectively, in the 3:13:2 structure, with the 2c sites in the latter being filled by B. The rare earth 1a site in the 1:5 splits into two crystallographically different sites, 1a and 2e, in the 3:13:2 structure.

In this contribution, we present results of powder neutron diffraction experiments and Density Functional Theory (DFT) calculations at the Local Spin Density Approximation (LSDA) and Generalized Gradient Approximation (GGA) levels performed on $Y_3T_{13}B_2$ and $Y_3Ni_{10}Co_3B_2$ compounds, T = Co, Ni. The effect of crystal structure details on the electronic structure and MAE of the 3:13:2 phases, with respect to the reference, extensively studied YCo_5 phase, is examined. The article is organized as follows. In Sec. II, we describe the conditions of the diffraction experiments, the data refinement strategy, and the computational details. The crystal structure parameters, the electronic structure, local magnetic moments, and the MAE results are reported in Sec. III. In Sec. IV, we discuss the magnetic anisotropy behavior in the itinerant electron systems studied in this work in relationship to the orbital magnetic moment anisotropy and available data from literature. The main results are summarized in Sec. V.

II. METHODS

A. Powder diffraction experiments

Samples with the nominal compositions $Y_3Ni_{13}B_2$, $Y_3Co_{13}B$ and $Y_3Ni_{10}Co_3B_2$ used in the present investigations were taken from batches of polycrystalline materials prepared as reported elsewhere.[36] These samples contained
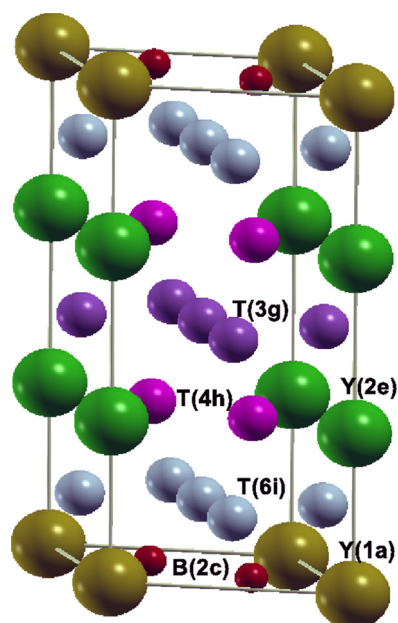

FIG. 1. The $Nd_3Ni_{13}B_2$-type crystal structure of $Y_3T_{13}B_2$, T = Co, Ni.

natural abundance boron. The ingots were coarsely crushed, then ground and sieved to obtain about 10 g of fine powders of each composition, with average grain size less than 20 μm.

Based on previously reported x-ray diffraction results,[36] which showed that $Y_3Co_{13}B_2$ consists of a mixture of phases, we carried out the neutron measurements only on the $Y_3Ni_{13}B_2$ and $Y_3Ni_{10}Co_3B_2$ samples, at the Institute Laue Langevin, Grenoble. The powders were enclosed in vanadium tubes of 6 mm in diameter and measured on the diffractometer D20 working at a wavelength of ~1.890 Å, over the angular range from 2° to 154°, with a step of 0.1°, in the temperature range 1.8–249 K. The sample with the nominal stoichiometry $Y_3Co_{13}B_2$ was crosschecked by scanning in a Bruker D501 x-ray diffractometer with Cu k_α radiation, at room temperature. The diffraction data were analyzed using the FullProf Suite[37] software package, following the general guidelines for structure refinement.[38] A linear absorption factor was used for the neutron data fitting process, in order to account for neutron absorption by the ^{10}B isotope present in the samples.[39]

In the analysis of the neutron diffraction patterns of $Y_3Ni_{13}B_2$ and $Y_3Ni_{10}Co_3B_2$, we firstly performed full refinements of the nuclear contributions at high temperature (233 K and 249 K), well above the magnetic ordering temperatures of the compounds (68 K and 170 K, respectively). Then, the lattice constants, zero shift, and atomic positions were refined at 1.8 K, maintaining all other fit parameters fixed to their high temperature values. Finally, the *ab initio* calculated magnetic moments were taken as initial parameters for the refinement of the magnetic contribution at 1.8 K, while maintaining all structural parameters fixed. We assumed a crystallographic-like magnetic unit cell and imposed the constraint of collinearity to the local magnetic moments.

B. Density functional theory calculations

Scalar relativistic and fully relativistic calculations were performed using the FPLO code[40–42] version 9. The code is based on the method of linear combination of nonorthogonal overlapping local orbitals and uses a full potential scheme, which allows to attain a high level of accuracy in total energy calculations. The fully relativistic mode is an implementation of the 4-component Kohn-Sham-Dirac theory and includes spin-orbit (SO) coupling and magnetic anisotropy.[42] The exchange and correlations potential was treated in the parameterizations of Perdew and Wang,[43] in the LSDA approach, and Perdew-Burke-Ernzerhof[44] (PBE), in the GGA approach. We carried out convergence tests of the total energy with the number of k-points integration in the Brillouin zone, using up to a $24 \times 24 \times 24$ grid (793 irreducible k-points from 13824) for the pure 3:13:2 phases and up to $36 \times 36 \times 36$ grid (2413 irreducible k-points from 46656) for YCo_5. The calculations on the chemically disordered $Y_3Ni_{10}Co_3B_2$ were performed on a $3 \times 1 \times 1$ supercell, with 54 atoms, using a coarser grid, up to $6 \times 6 \times 6$ (216 k-points in the irreducible BZ). Consequently, the error in the total energy values obtained in this work is 10^{-4} eV, at most.

In the fully relativistic mode, the calculations were performed with and without using an orbital polarization correction (OPC) applied to Co and Ni 3d states. As a result of test calculations performed on YCo$_5$, we chose the spin dependent OPC implementation.[15,45] The application of OPC to the Y 4d states had no effect.

We performed the structural optimization of the 3:13:2 compounds, with the internal coordinates relaxed to a maximum force left on an atom of about 0.05 eV/Å. The calculations on YCo$_5$ were carried out at the experimental lattice constants[46] in order to allow a comparison of the present MAE results with reference data. In this work, the total density of states (DOS) is given in (states/eV/cell) and the element and site-projected DOS are in (states/eV/at.). The Fermi energy is set at 0 eV.

III. RESULTS

A. Crystal structure

The experimental and calculated neutron diffraction patterns of Y$_3$Ni$_{13}$B$_2$ and Y$_3$Ni$_{10}$Co$_3$B$_2$ at 1.8 K are plotted in Fig. 2. Only the markers corresponding to the refinement of the nuclear contribution are shown for Y$_3$Ni$_{13}$B$_2$, as no magnetic contribution could be observed when comparing the data collected at 233 K to the data at 1.8 K. We recall that a magnetic moment of only 0.25–0.30 μ_B/f.u. at 5 T and 5 K was previously determined[36] by magnetization measurements in Y$_3$Ni$_{13}$B$_2$, which is beyond the resolution of the present experimental data. In the case of Y$_3$Ni$_{10}$Co$_3$B$_2$, both contributions, nuclear and magnetic, were included in the refinement. The corresponding crystal structure parameters are listed in Table I, together with the refined x-ray diffraction results for Y$_3$Co$_{13}$B$_2$ at room temperature. The parameters of Y$_3$Ni$_{13}$B$_2$ and Y$_3$Ni$_{10}$Co$_3$B$_2$ at 233 K and 249 K, respectively, are also listed between braces, to allow a comparison between structural data at low and high temperature. With respect to a uniform Co distribution in Y$_3$Ni$_{10}$Co$_3$B$_2$, i.e., 23.1% Co atoms occupying each of the 3d metal sites, Co shows a strong preference for the 3g sites (34%), avoids 4h sites (18%) and to a less extent the 6i sites (22%). The refined phase contents in the Y$_3$Ni$_{13}$B$_2$ and Y$_3$Ni$_{10}$Co$_3$B$_2$ samples amount to (88.8 ± 1.5, 7.8 ± 0.4, 3.4 ± 0.3) and (100, 0, 0) wt. % for the (3:13:2, 1:4:1, 1:5) phases, respectively.

TABLE I. The lattice constants, a and c; their ratio, c/a; the internal coordinates, z; the unit cell volume, $V_{u.c.}$; the figures of merit χ^2; and Bragg reliability factor, R_B, for Y$_3$Ni$_{13}$B$_2$ and Y$_3$Ni$_{10}$Co$_3$B$_2$ obtained from the refinement of the nuclear contributions to the neutron diffraction patterns at 1.8 K, and for Y$_3$Co$_{13}$B$_2$ from the refinement of the x-ray diffraction pattern, at room temperature. The fractional occupancies for Ni and Co at. the 6i, 4h and 3g sites in Y$_3$Ni$_{10}$Co$_3$B$_2$ are also given.

	Y$_3$Ni$_{13}$B$_2$	Y$_3$Ni$_{10}$Co$_3$B$_2$	Y$_3$Co$_{13}$B$_2$
a (Å)	4.9524(1)[a]	4.9610(2)	5.0063(3)
	{4.9592(1)}[b]	{4.9698(2)}	
c (Å)	10.9061(5)	10.9053(6)	10.853(1)
	{10.9195(4)}	{10.9155(7)}	
z, 6i	0.1345(3)	0.1340(2)	0.1441(9)
	{0.1345(2)}	{0.1342(3)}	
z, 4h	0.3181(6)	0.3189(4)	0.328(2)
	{0.3181(5)}	{0.3190(5)}	
z, 2e	0.3282(9)	0.3283(7)	0.316(1)
	{0.3282(7)}	{0.3276(8)}	
6i occ.		Ni, 0.78(1) {0.80(1)}	
		Co, 0.22(1) {0.20(1)}	
4h occ.		Ni, 0.82(1) {0.83(1)}	
		Co, 0.18(1) {0.17(1)}	
3g occ.		Ni, 0.66(1) {0.66(1)}	
		Co, 0.34(1) {0.34(1)}	
c/a	2.202	2.198	2.168
	{2.202}	{2.196}	
$V_{u.c.}$ (Å^3)	231.65(1)	232.44(1)	235.57(4)
	{232.57(1)}	{233.49(2)}	
χ^2	3.93	13.9	2.72
	{6.94}	{1.48}	
R_B	5.66	6.34	6.04
	{5.04}	{7.51}	

[a]Between parentheses: standard deviations.
[b]Between braces: the values at 233 K for Y$_3$Ni$_{13}$B$_2$ and at 249 K for Y$_3$Ni$_{10}$Co$_3$B$_2$.

The presently refined values of the lattice constants of Y$_3$Co$_{13}$B$_2$ compound are in fair agreement with the previously reported ones.[36]

In the case of the Y$_3$Ni$_{10}$Co$_3$B$_2$, one has to build a 3 × 1 × 1 supercell starting from the structural data determined at 1.8 K, see Table I, in order to match the real composition and carry out the calculations. Using the refined Ni and Co fractional occupancies at the 6i, 4h, and 3g sites, one
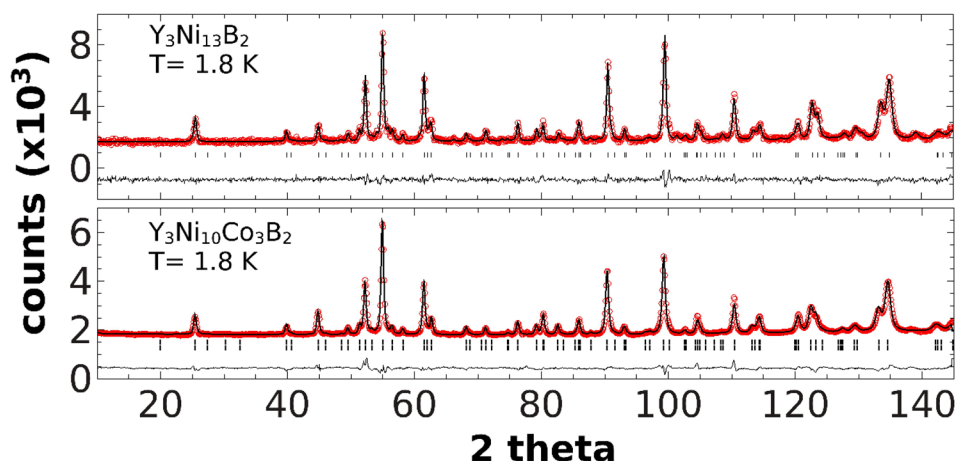

FIG. 2. Experimental and calculated 1.8 K neutron diffraction patterns of Y$_3$Ni$_{13}$B$_2$ and Y$_3$Ni$_{10}$Co$_3$B$_2$.

obtains the composition $Y_9Ni_{29.82}Co_{9.18}B_6$ ($Y_3Ni_{9.94}Co_{3.06}B_2$) which closely matches the nominal 3:10:3:2 stoichiometry. In this structural model, we have assumed the random distribution of 4, 2, and 3 Co atoms at the $3 \times$ (6i, 4h and 3g) sites, respectively.

B. Density functional theory study

1. $Y_3T_{13}B_2$ compounds, T = Co, Ni

Firstly, we performed scalar-relativistic LSDA calculations to structurally optimize the pure $Y_3T_{13}B_2$ compounds, starting from the experimental data displayed in Table I. The $E(V)$ curves obtained by isotropically varying the unit cell volume were fitted to the recently parameterized form[47] of the Murnaghan equation of state. Furthermore, the c/a ratio was optimized at the equilibrium volume, and then the internal coordinates z were relaxed. The structural parameters at equilibrium are listed in Table II. One may note that the calculated lattice constants are by 2–3% smaller than their experimental values given in Table I, which is due to the usual overestimation of the binding energy in LDA.[48] The larger differences in the case of $Y_3Co_{13}B_2$ than for the nickel compound reflect a contribution from the crystal thermal expansion, given the different temperatures of diffraction data acquisition (RT for Co and 1.8 K for Ni). Also, the internal coordinates z show larger variations in the case of $Y_3Co_{13}B_2$ than for $Y_3Ni_{13}B_2$, which may be related to a significant change in the c/a ratio for the Co compound, from 2.168 in experiment to 2.197 after the geometry optimization process. Meanwhile, c/a varies only slightly for T = Ni, from 2.202 to 2.204, see Tables I and II.

Then, LSDA scalar relativistic and fully relativistic calculations were performed on $Y_3T_{13}B_2$ at the equilibrium structural parameters, listed in Table II. In the case of $Y_3Ni_{13}B_2$, we also conducted extensive calculations assuming several collinear spin configurations of antiferromagnetically coupled ferromagnetic Ni planes, with the quantization axes along [001] and [100] directions, to probe the eventual occurrence of an AFM ground state.[36] However, ferromagnetism was found in each considered case, which suggests that the experimentally observed AFM-type magnetic behavior accompanying the ferromagnetic mode may be due to disordered local magnetic moments.

The total element and site-projected densities of states of $Y_3Ni_{13}B_2$ and $Y_3Co_{13}B_2$ are plotted in Figs. 3 and 4,
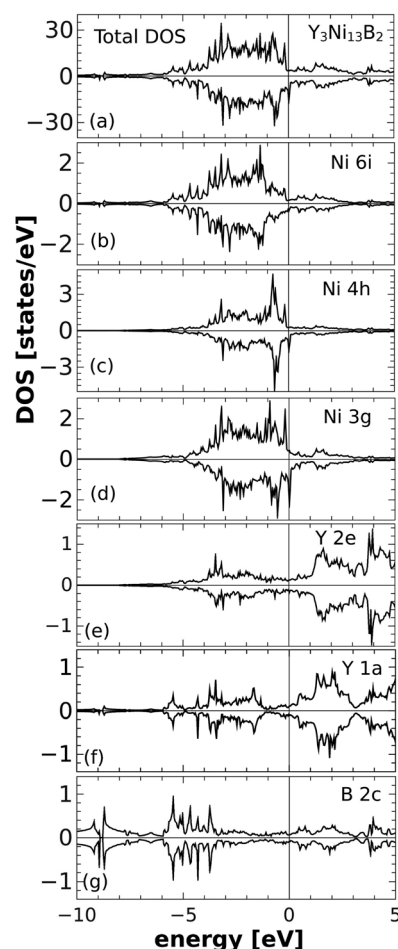

FIG. 3. Total and site-resolved DOS plots of $Y_3Ni_{13}B_2$.

respectively. The total DOS plots, see Figs. 3(a) and 4(a), show ferromagnetic ground states for both compounds, with the top edge of the spin up subband just below the Fermi energy, similar to the case of YCo_5, for which the total DOS is depicted in Fig. 5.

The total spin magnetic moment, M_s, takes the values 1.03 μ_B/f.u. for $Y_3Ni_{13}B_2$, 11.80 μ_B/f.u. for $Y_3Co_{13}B_2$, and 6.99 μ_B/f.u. for YCo_5. The on-site spin and orbital magnetic moments are collected in Table III. In $Y_3Co_{13}B_2$, the largest magnetic moments, both spin and orbital, reside at the 4h site and the lowest ones at the 6i site which has a boron nearest neighbor at very short distance, 2.042 Å. Thus, the low magnetic state at the Co 6i site may be ascribed to the Co 3d states overlap with the B 2p states, particularly at energies below -6 eV, see Figs. 4(b) and 4(g). This overlap is responsible for the tail in the DOS of Co 6i down to about -9 eV, feature which is not observed in the DOS plots of Co 4 h and Co 3 g, see Figs. 4(c) and 4(d). A tail down to -10 eV may also be observed in the DOS of Y 1a in Fig. 4(f), which has a boron nearest neighbor at 2.787 Å, due to Y 4d states overlap with B 2p states. Similar features may also be observed in the DOS plots of the $Y_3Ni_{13}B_2$ compound, shown in Fig. 3. Rather surprisingly, in this case, the calculations predict the largest spin and orbital magnetic moments at the Ni 3g site.

A small, negative spin magnetic moment is calculated at the Y sites, which is larger in the Co compound than in the

TABLE II. Equilibrium crystal structure parameters of $Y_3T_{13}B_2$, T = Co, Ni, and $Y_3Ni_{9.94}Co_{3.06}B_2$. Between parentheses: the percentage variations of the parameters.

	$Y_3Ni_{13}B_2$	$Y_3Ni_{9.94}Co_{3.06}B_2$	$Y_3Co_{13}B_2$
a (Å)	4.8386 (−2.30%)	4.8342 (−2.56%)	4.8281 (−3.56%)
c (Å)	10.6652 (−2.21%)	10.6267 (−2.55%)	10.6067 (−2.27%)
z, 6i	0.1354 (+0.7%)	0.1381 (+3.0%)	0.1407 (−2.4%)
z, 4h	0.3192 (+0.3%)	0.3285 (+3.0%)	0.3205 (−2.3%)
z, 2e	0.3279 (−0.1%)	0.3383 (+3.0%)	0.3242 (+2.6%)
c/a	2.204	2.198	2.197
$V_{u.c.}$ (Å^3)	216.24 (−6.65%)	215.07 (−7.47%)	214.12 (−9.11%)

FIG. 4. Total and site-resolved DOS plots of $Y_3Co_{13}B_2$.

LSDA. The GGA total DOS plots, not shown here, of the compounds under discussion, bear all the features also described in the LSDA approach.

2. $Y_3Ni_{9.94}Co_{3.06}B_2$ compound

The LSDA total DOS and Co site-resolved DOS obtained in supercell calculations at the equilibrium structural parameters are plotted in Figs. 6(a)–6(d). The minority spin subband in the total DOS, Fig. 6(a), is shifted toward lower energy comparing with $Y_3Co_{13}B_2$, as a result of 3d band filling. The site averaged Ni and Co spin and orbital magnetic moments are listed in Table III. Co shows depressed spin magnetic moments relative to the values in $Y_3Co_{13}B_2$. The largest spin magnetic moments are localized at the Co 4h and Ni 3g sites, similarly to the 3d metal behavior in the pure compounds, and the total spin moment is $M_s = 3.69 \, \mu_B$/f.u. The small, negative magnetic moments due to the polarization of the conduction electrons at yttrium sites take intermediate values between those in the pure Ni and Co compounds. Figure 7 displays the total spin density isosurfaces drawn for each layer in the $Y_3Ni_{9.94}Co_{3.06}B_2$ unit cell. It is worth noting that Ni sites with Co nearest neighbors show an enhanced magnetic moment with respect to Ni in a less magnetic local environment.

The Co and Ni site-averaged magnetic moments calculated for $Y_3Ni_{9.94}Co_{3.06}B_2$, see Table III, were used as initial parameters in the fitting of the magnetic contribution to the neutron diffraction pattern of $Y_3Ni_{10}Co_3B_2$ shown in Fig. 2. The refined, site averaged magnetic moments are 0.39, 1.42, and 1.38 μ_B/at. for Co, and 0.04, 0.21, and 0.29 μ_B/at. for Ni, at the 6i, 4h, and 3g sites, respectively. Using the fractional occupancies given in Table I, the average magnetic moment values of 0.98 μ_B/Co at. and 0.15 μ_B/Ni at. are obtained, in excellent agreement with the average calculated moments (including spin and orbital) of 1.03 μ_B/Co at. and 0.15 μ_B/Ni at.

3. Magnetocrystalline anisotropy energy

Fully relativistic calculations, using a rigid splitting of the spin-up and spin-down states, were performed on the three compounds studied in this work, as well as on YCo_5, with the quantization axis along the [001] and [100] directions, in order to evaluate the orbital magnetism, the anisotropy of the magnetic moments and the MAE. The values of the orbital magnetic moment, obtained in calculations with orbital polarization correction, are listed in Table III. As a result of the relativistic symmetry reduction when the quantization axis is set along the [100] direction for $Y_3T_{13}B_2$, the 3g and 6i sites each split into two subgroups with intensity two to one, similarly to the 3g site in YCo_5.[18] No relativistic symmetry reduction takes place in the case of $Y_3Ni_{9.94}Co_{3.06}B_2$ in the calculation along the [100] direction because the supercell was treated in the P1 space group.

Whereas no significant orbital magnetic moment resides on Ni, a considerable orbital moment is calculated for Co 4h and Co 3g sites, with a particularly large orbital moment anisotropy at the Co 4h site, see Table III. We emphasize that these results are supported by the

Ni one, and also larger at the Y 2e site than at the Y 1a site. This is consistent with a negative polarization of the valence electrons at the Y sites by the neighboring Co magnetic moments due to Y 4d-Co 3d states mixing, as is usually found in yttrium 3d transition metal compounds.[16–18,49–52]

Although the LSDA has proven to describe remarkably accurate many properties of weakly correlated electron systems, we cross-checked the present LSDA results by using a "beyond-LSDA" method, the GGA, as implemented in the FPLO9 code. In the GGA approach, a gradient expansion of the exchange and correlation energy is introduced, which provides an enhancement factor, function of density and scaled gradient, over the LDA exchange.[53] The GGA values of the spin and orbital magnetic moments are also listed in Table III. One may observe that GGA-PBE predicts a slightly enhanced spin ferromagnetism with respect to the
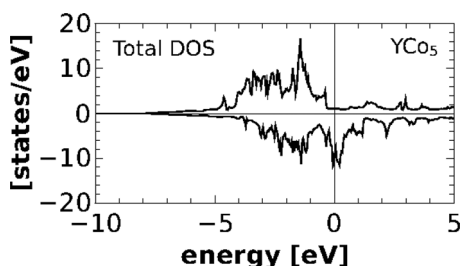

FIG. 5. LSDA total DOS plot of YCo_5.

TABLE III. On-site spin, m_s, and orbital, m_l, magnetic moments in $Y_3T_{13}B_2$, T = Co, Ni, $Y_3Ni_{9.94}Co_{3.06}B_2$, and YCo_5 (this work). The values at the experimental structural parameters of $Y_3Ni_{9.94}Co_{3.06}B_2$ are also given.

				m_s ($\mu_B/at.$)		
Compound		T, 6i	T, 4h	T, 3g	Y, 2e	Y, 1a
$Y_3Ni_{13}B_2$[a]		0.01	0.12	0.20	−0.02	−0.01
		(0.01)	(0.16)	(0.27)	(−0.04)	(−0.01)
$Y_3Co_{13}B_2$[a]		0.51	1.36	1.33	−0.21	−0.12
		(0.68)	(1.45)	(1.40)	(−0.26)	(−0.17)
YCo_5[b]		...	1.45	1.47	−0.31	
$Y_3Ni_{9.94}Co_{3.06}B_2$[a,c]		Co Ni	Co Ni	Co Ni		
Equi. structure		0.26 0.04	1.30 0.20	1.25 0.28	−0.08	−0.02
Exp. structure		0.39 0.04	1.45 0.22	1.39 0.30	−0.09	−0.03
		(0.49 0.04)	(1.51 0.24)	(1.47 0.32)	(−0.12)	(−0.05)
	q-axis			m_l ($\mu_B/at.$)		
$Y_3Ni_{13}B_2$	[001]	0.00	0.01	0.02	0.00	0.00
	[100]	0.00, 0.00	0.02	0.03, 0.03	0.00	0.00
$Y_3Co_{13}B_2$[a]	[001]	0.04	0.30	0.22	0.03	0.00
		(0.06)	(0.29)	(0.22)	(0.03)	(0.00)
	[100]	0.04, 0.09	0.19	0.16, 0.23	0.00	0.00
		(0.07, 0.12)	(0.19)	(0.17, 0.23)	(0.01)	(0.01)
YCo_5[b]	[001]		0.37	0.30	0.04	
	[100]		0.27	0.19, 0.33	0.02	
$Y_3Ni_{9.94}Co_{3.06}B_2$[c]		Co Ni	Co Ni	Co Ni		
Equi. structure	[001]	0.03 0.00	0.50 0.02	0.20 0.03	0.01	0.00
	[100]	0.02 0.00	0.20 0.03	0.17 0.03	0.00	0.00
Exp. structure	[001]	0.05 0.00	0.74 0.03	0.25 0.04	0.01	0.00
	[100]	0.05 0.00	0.33 0.04	0.20 0.04	0.00	0.00

[a]Between round brackets: the GGA-PBE spin and orbital magnetic moments.
[b]The sites 4h, 3g, and 2e in the $Nd_3Ni_{13}B_2$-type structure are crystallographically equivalent to the sites 2c, 3g, and 1a, respectively, in the $CaCu_5$-type structure.
[c]Co and Ni site-averaged magnetic moments.

GGA-PBE calculations. MAE was evaluated as the difference between the total energy values obtained in SCF calculations along the 001 and 100 axes with the spin-orbit coupling switched on, $E_T(q100)–E_T(q001)$. The LSDA results are listed in Table IV, together with reference data for YCo_5. A somewhat reduced MAE value, 0.27 meV/Co at. (2.62 MJ/m³) was derived for $Y_3Co_{13}B_2$ in GGA-PBE calculations.
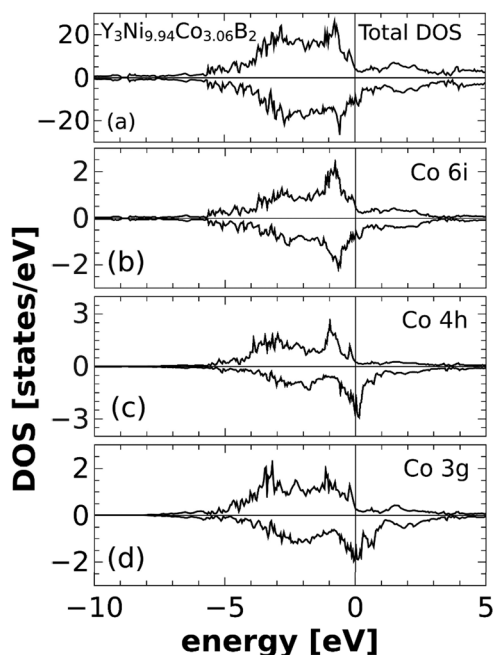

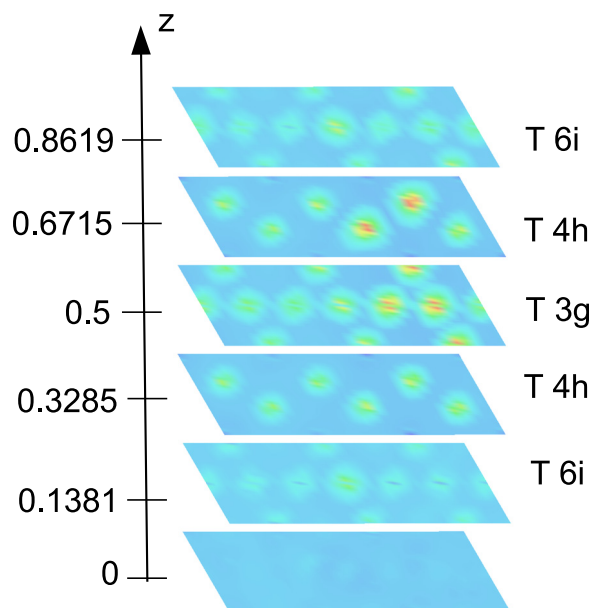FIG. 6. Total and site-resolved Co DOS plots of $Y_3Ni_{9.94}Co_{3.06}B_2$.

FIG. 7. Total spin density isosurfaces in the (00z) planes of the $Y_9Ni_{29.82}Co_{9.18}B_6$ supercell.

TABLE IV. Magnetocrystalline anisotropy energy, LSDA results. The values at the experimental structural parameters of $Y_3Ni_{9.94}Co_{3.06}B_2$ are also given.

Compound	k-points mesh	MAE		
		meV/f.u.	meV/3d at.	MJ/m^3
$Y_3Ni_{13}B_2$[a]	$16 \times 16 \times 16$	0.66	0.05	0.49
	$24 \times 24 \times 24$	0.58	0.04	0.43
$Y_3Co_{13}B_2$	$16 \times 16 \times 16$	5.84	0.45	4.37
	$24 \times 24 \times 24$	5.74	0.44	4.30
$Y_3Ni_{9.94}Co_{3.06}B_2$[b]				
Equi. structure	$4 \times 4 \times 4$	3.91	1.28	2.9
Exp. structure	$3 \times 3 \times 3$	7.45	2.43	5.1
	$4 \times 4 \times 4$	8.11	2.65	5.6
YCo_5, this work	$24 \times 24 \times 24$	5.23	1.05	9.98
	$36 \times 36 \times 36$	5.14	1.03	9.80
YCo_5, calculations		0.60[c]	0.12	1.14
		4.4[d]	0.88	8.40
		1.51[e]	0.30	2.88
YCo_5, exp.		3.86[f]	0.77	7.38

[a]In-plane magnetic anisotropy.
[b]Values in meV/Co at.
[c]Reference 16, LMTO-ASA.
[d]Reference 17, LCAO, SO coupling and OP correction.
[e]Reference 18, LAPW, $p_{1/2}$ extension, GGA and nonspherical corrections.
[f]Reference 9.

IV. DISCUSSION

A survey of the orbital magnetic moment values displayed in Table III, lower section, shows that Co 6i has an orbital magnetic moment smaller by one order of magnitude than Co 4h and Co 3g, and no orbital magnetic moment anisotropy. In contrast, there is considerable orbital magnetization and OMA at the Co 4h and 3g sites in the 3:13:2 structure, which are crystallographically related to the 2c and 3g sites in the 1:5 structure. Moreover, the changes in the orbital moment values are similar when switching the quantization axis from [001] to [100] direction, for these sites, in both types of structures.

The MAE results listed in Table IV show that (i) for the calculations performed in this work, increasing the k mesh finesse determines a variation of 0.1 meV/f.u. in the magnetic anisotropy energy, excepting the larger difference, of 0.6 meV/f.u., in the case of the supercell calculations at the experimental lattice parameters; a denser grid should be used for the disordered compound, but the computational effort is substantial, (ii) in-plane magnetic anisotropy is predicted for $Y_3Ni_{13}B_2$, while both $Y_3Co_{13}B_2$ and $Y_3Ni_{9.94}Co_{3.06}B_2$ exhibit uniaxial anisotropy, (iii) the calculated magnetic anisotropy energy of $Y_3Co_{13}B_2$ superstructure is about one half of that calculated for YCo_5, using the same formalism and code, (iv) the magnetocrystalline anisotropy energy of the mixed compound, at the equilibrium structure, is considerable, having in view the moderate substitution rate (23 at.% Co); a comparison between the MAE values (in MJ/m^3) calculated at the experimental volume and at equilibrium volume reveals the strong dependence on $V_{u.c.}$: an increase by 7.47% in volume determines an increase by about 93% in MAE, and

(v) the MAE of YCo_5 calculated in this work is overestimated with respect to the experimental value,[9] 3.8 meV, which may be associated with the effect of the empirical OPC used.[45]

The in-plane magnetic anisotropy predicted for $Y_3Ni_{13}B_2$ should be considered only qualitatively, due to our assumption of collinear ferromagnetic Ni magnetic moments arrangement. For $Y_3Co_{13}B_2$ and $Y_3Ni_{9.94}Co_{3.06}B_2$, the calculations predict considerable magnetic anisotropy energy, which we associate with both the large orbital magnetic moment values and large OMA at the Co 4h and Co 3g sites, see Table III. Previously, a substantial MAE increase when increasing Co concentration was experimentally determined for $Sm(Ni_{1-x}Co_x)_5$ at 4.2 K.[54] Also, an increase in the MAE was determined by DFT + U calculations in Fe doped $SmCo_5$ and YCo_5.[19] In both series, MAE increases by about 1 meV/f.u. for 3–4% Fe in $SmCo_5$ and 6–7% Fe in YCo_5, then decreases rapidly with increasing the Fe concentration. The predicted maximum in MAE was related to Fe concentrations, where the Fermi level moves to the top of the Co 2c density of states for the magnetic field applied along the [100] direction.[19]

An examination of the total DOS plots displayed in Figs. 3(a), 4(a), and 6(a) reveals that the T-3d band edge in the majority band is close, at about 0.1–0.2 eV below the Fermi energy, similarly to the Co-3d band edge in YCo_5, see Fig. 5(a). Recalling that an electronic topological (Lifshitz) transition of magnetoelastic origin was previously reported[55,56] in YCo_5, one may expect a collapse of the magnetization or a crossover to a low-moment state to occur at rather low pressure in the $Y_3T_{13}B_2$ and $Y_3Ni_{10}Co_3B_2$ compounds. However, the $Y_3Co_{13}B_2$ compound could be studied only in theory until it will be synthesized as a pure phase.

V. CONCLUSIONS

The main results of our work, obtained by LSDA-GGA calculations and powder neutron diffraction experiments, may be summarized as follows. The local spin and orbital magnetic moments, as well as the magnetocrystalline anisotropy energy of $Y_3Ni_{13}B_2$, $Y_3Co_{13}B_2$ and $Y_3Ni_{10}Co_3B_2$ compounds were evaluated. The calculations suggest an in-plane magnetic anisotropy in $Y_3Ni_{13}B_2$, which, under the stated assumptions, is in line with experimental results indicating an uncompensated AFM state. Since the calculations performed on different configurations of antiferromagnetically coupled ferromagnetically ordered Ni planes in $Y_3Ni_{13}B_2$ gave no stable energy minimum solution, we suggest that the experimentally observed uncompensated AFM behaviour may be due to Ni disordered local moments. A close relationship between the magnitude of the orbital magnetic moment and OMA, on one side, and the magnetocrystalline anisotropy energy, on the other, is evidenced in the 3:13:2 itinerant electron systems. The density of states plots show that the B 2p-T 3d states mixing decreases the T 3d spin and especially the 3d orbital magnetic moment. It is for the first time, to our knowledge, when the local magnetic moments and MAE of the Y based 3:13:2 phases are evaluated.

ACKNOWLEDGMENTS

[1]P. Rogl, "Phase equilibria in ternary and higher order systems with rare earth elements and boron," in *Handbook on the Physics and Chemistry of Rare Earths*, edited by K. A. Gschneidner, Jr. and L. Eyring (Elsevier Science Publishing B.V., North-Holland, 1984), Vol. 6, p. 470.

[2]E. Parthé and B. Chabot, "Crystal structures and crystal chemistry of ternary rare earth-transition metal borides, silicides and homologues," in *Handbook on the Physics and Chemistry of Rare Earths*, edited by K. A. Gschneidner, Jr. and L. Eyring (Elsevier Science Publishing B.V., North-Holland, 1984), Vol. 6, p. 113.

[3]K. J. Strnat and R. M. W. Strnat, J. Magn. Magn. Mater. **100**, 38 (1991).

[4]J. J. M. Franse and R. J. Radwanski, in *Handbook of Magnetic Materials*, edited by K. H. J. Buschow (Elsevier, North Holland, Amsterdam, 1993), Vol. 7, p. 307.

[5]O. Gutfleisch, "High-temperature samarium cobalt permanent magnets," in *Nanoscale Magnetic Materials and Applications*, edited by J. P. Liu, E. Fullerton, O. Gutfleisch, and D. J. Sellmyer (Springer, 2009), p. 337.

[6]G. C. Hadjipanayis, J. F. Liu, A. Gabay, and M. Marinescu, J. Iron Steel Res. Int. **13**(Suppl. 1), 12 (2006).

[7]C. B. Rong, N. Poudyal, X. B. Liu, Y. Zhang, M. J. Kramer, and J. P. Liu, Appl. Phys. Lett. **101**, 152401 (2012).

[8]P. Chowdhury, M. Krishnan, H. C. Barshilia, D. V. S. Rao, D. Kumar, and C. Shivakumara, J. Magn. Magn. Mater. **342**, 74 (2013).

[9]J. M. Alameda, D. Givord, R. Lemaire, and Q. Lu, J. Appl. Phys. **52**, 2079 (1981).

[10]S. G. Sankar, V. U. S. Rao, E. Segal, W. E. Wallace, W. G. D. Frederick, and H. J. Garrett, Phys. Rev. B **11**, 435 (1975).

[11]J. Schweizer and F. Tasse, J. Phys. F: Met. Phys. **10**, 2799 (1980).

[12]R. L. Streever, Phys. Rev. B **19**, 2704 (1979).

[13]M. Richter, "Density functional theory applied to 4f and 5f elements and metallic compounds," in *Handbook of Magnetic Materials*, edited by K. H. J. Buschow (North-Holland, Amsterdam, 2001), Vol. 13, p. 87.

[14]M. Yamaguchi and S. Asano, J. Magn. Magn. Mater. **168**, 161 (1997).

[15]L. Nordström, M. S. S. Brooks, and B. Johansson, J. Phys.: Condens. Matter **4**, 3261 (1992).

[16]G. H. O. Daalderop, P. J. Kelly, and M. F. J. Schuurmans, Phys. Rev. B **53**, 14415 (1996).

[17]L. Steinbeck, M. Richter, and H. Eschrig, Phys. Rev. B **63**, 184431 (2001).

[18]P. Larson and I. I. Mazin, J. Magn. Magn. Mater. **264**, 7 (2003); J. Appl. Phys. **93**, 6888 (2003).

[19]P. Larson, I. I. Mazin, and D. A. Papaconstantopoulos, Phys. Rev. B **69**, 134408 (2004).

[20]I. Opahle, M. Richter, M. D. Kuz'min, U. Nitzsche, K. Koepernik, and L. Schramm, J. Magn. Magn. Mater. **290**, 374 (2005).

[21]C. Chacon and O. Isnard, J. Appl. Phys. **89**, 71 (2001).

[22]C. V. Colin, O. Isnard, and M. Guillot, J. Alloys Compd. **505**, 11 (2010).

[23]C. Chacon and O. Isnard, J. Phys.: Condens. Matter **13**, 5841 (2001).

[24]C. Chacon and O. Isnard, Appl. Phys. A **74**(1), S831 (2002).

[25]O. Isnard, M. D. Kuz'min, M. Richter, M. Loewenhaupt, and R. Bewley, J. Appl. Phys. **104**, 013922 (2008).

[26]C. Chacon, O. Isnard, L. Chioncel, C. Giorgetti, F. Baudelet, and E. Dartyge, J. Magn. Magn. Mater. **242–245**, 861 (2002).

[27]D. Music and J. M. Schneider, J. Phys.: Condens. Matter **18**, 4071 (2006).

[28]Y. Chen, Q. L. Liu, J. K. Liang, X. L. Chen, B. G. Shen, and F. Huang, Appl. Phys. Lett. **74**, 856 (1999).

[29]Y. Chen, X. Li, X. L. Chen, J. K. Liang, G. H. Rao, B. G. Shen, Q. L. Liu, L. P. Jin, and M. Z. Wang, Chem. Mater. **12**, 1240 (2000).

[30]Y. Chen, J. K. Liang, X. L. Chen, Q. L. Liu, B. G. Shen, and Y. P. Shen, J. Phys.: Condens. Matter **11**, 8251 (1999).

[31]Y. Chen, X. Li, J. K. Liang, X. L. Chen, B. G. Shen, G. H. Rao, and Q. L. Liu, IEEE Trans. Magn. **36**, 2037 (2000).

[32]N. Plugaru, J. Rubín, J. Bartolomé, and C. Piquer, J. Magn. Magn. Mater. **290–291**, 1563 (2005).

[33]N. Plugaru, J. Rubín, J. Bartolomé, J. Campo, G. J. Cuello, M. Tovar, and O. Prokhnenko, J. Magn. Magn. Mater. **316**, e438 (2007).

[34]A. Kowalczyk, A. Szajek, G. Chełkowska, and T. Toliński, Solid State Commun. **132**, 225 (2004).

[35]N. M. Hong, H. Michor, M. Vybornov, T. Holubar, P. Hundegger, W. Perthold, G. Hilscher, and P. Rogl, Physica C **227**, 85 (1994).

[36]N. Plugaru, J. Rubín, J. Bartolomé, and V. Pop, Phys. Rev. B **71**, 024433 (2005).

[37]J. Rodriguez-Carvajal, "FULLPROF: A program for Rietveld refinement and pattern matching analysis," in *Powder Diffraction, Satellite Meeting of the XV Congress of the International Union of Crystallography, Toulouse, 16–19 July* (1990); Physica B **192**, 55 (1993).

[38]L. B. McCusker, R. B. Von Dreele, D. E. Cox, D. Louër, and P. Scardi, J. Appl. Cryst. **32**, 36 (1999).

[39]http://www.ncnr.nist.gov/instruments/bt1/neutron.html

[40]K. Koepernik and H. Eschrig, Phys. Rev. B **59**, 1743 (1999).

[41]I. Opahle, K. Koepernik, and H. Eschrig, Phys. Rev. B **60**, 14035 (1999).

[42]H. Eschrig, M. Richter, and I. Opahle, "Relativistic solid state calculations," in *Relativistic Electronic Structure Theory, Part 2: Applications*, edited by P. Schwerdtfeger, Theoretical and Computational Chemistry Vol. 14 (Elsevier B.V., 2004), Chap. 12, p. 723.

[43]J. P. Perdew and Y. Wang, Phys. Rev. B **45**, 13244 (1992).

[44]J. P. Perdew, K. Burke, and M. Ernzerhof, Phys. Rev. Lett. **77**, 3865 (1996).

[45]H. Eschrig, M. Sargolzaei, K. Koepernik, and M. Richter, Europhys. Lett. **72**, 611 (2005).

[46]J. H. Wernick and S. Geller, Acta Crystallogr. **12**, 662 (1959).

[47]V. Tyuterev and N. Vast, Comput. Mater. Sci. **38**, 350 (2006).

[48]J. Kohanoff, *Electronic Structure Calculations for Solids and Molecules: Theory and Computational Methods* (Cambridge University Press, 2006).

[49]E. Krén, J. Schweizer, and F. Tasset, Phys. Rev. **186**, 479 (1969).

[50]J. G. M. Armitage, T. Dumelow, P. C. Riedi, and J. S. Abell, J. Phys.: Condens. Matter **1**, 3987 (1989).

[51]R. Coehoorn, J. Magn. Magn. Mater. **99**, 55 (1991).

[52]H. Yamada, K. Terao, H. Nakazawa, I. Kitagawa, N. Suzuki, and H. Ido, J. Magn. Magn. Mater. **183**, 94 (1998).

[53]M. Fuchs, "Comparison of exchange-correlation functionals: From LDA to GGA and beyond density-functional theory calculations for modeling materials and bio-molecular properties and functions," in *A Hands-On Computer Course, 30 October–5 November 2005, IPAM, UCLA, Los Angeles, USA* (2005).

[54]A. S. Ermolenko, E. I. Zabolotski, and A. V. Korolev, Fiz. Met. Metalloved. **41**, 960 (1976).

[55]H. Rosner, D. Koudela, U. Schwarz, A. Handstein, M. Hanfland, I. Opahle, K. Koepernik, M. D. Kuz'min, K.-H. Müller, J. A. Mydosh, and M. Richter, Nat. Phys. **2**, 469 (2006).

[56]D. Koudela, U. Schwarz, H. Rosner, U. Burkhardt, A. Handstein, M. Hanfland, M. D. Kuz'min, I. Opahle, K. Koepernik, K.-H. Müller, and M. Richter, Phys. Rev. B **77**, 024411 (2008).